https://doi.org/10.5194/wes-2026-133
Preprint. Discussion started: 30 July 2026

Low-Frequency Fatigue monitoring using nacelle-mounted accelerometers

Mustapha Chaar[1,2] Wout Weijtjens[1], Christof Devriendt[1]

[1]Department of Applied Mechanics, OWI-LAB, Vrije Universiteit Brussel, Brussels, 1050, Belgium
[2]24SEA, Brussels, 1000, Belgium

Correspondence to: Mustapha Chaar (Mustapha.chaar@vub.be)

Abstract. Thrust loading on wind turbines causes quasi-static loading that ultimately introduces fatigue loading on the turbine. Monitoring these quasi-static loads is relevant for assessing the residual lifetime of the asset. However, installing strain gauges on all assets is practically and economically infeasible; only a subset of turbines, referred to as fleet leaders, are instrumented to this level. Interestingly, these quasi-static loads also result in a temporary inclination or tilt of the tower, which can be picked up by accelerometers or inclinometers installed on the tower or nacelle. This paper proposes using gravity-sensitive tri-axial MEMS accelerometers placed in the nacelle to estimate the inclination and load characteristics of a fleet of turbines. To do this accurately, the MEMS sensor needs to be *calibrated* to offset installation errors and compensate for the turbines' permanent inclination. For this purpose, long-term data from the MEMS accelerometer are processed, and the constituting offsets are estimated. After calibration, the quasi-static angles induced by loading can be estimated from the accelerometer. The derived load characteristics can then be used to extrapolate bending moments from fully instrumented fleet-leader turbines to the remainder of the wind farm. The bending moment is then used to assess damage-equivalent moments, and it was found that the accelerometer produces damage estimates similar to those obtained from strain gauges. Thus, the approach enables scalable and cost-effective farmwide load monitoring.

1 Introduction

1.1 Motivation

Wind energy design is often driven by fatigue considerations, with the Fatigue Limit State (FLS) often being a design driver for (offshore) wind turbines in operation today (Vorpahl et al., 2013). With growing interest in extending the lifetime of these current assets, there is considerable interest in monitoring fatigue loads over the lifetime. In particular, it is important to ensure that the FLS criterion is not reached within the (extended) lifetime for the irreplaceable substructure (Wilkie and Galasso, 2021). Wind turbine substructures are typically designed to be inspection-free. Moreover, detecting fatigue cracks on these massive and, for offshore, partially submerged structures is deemed infeasible. As such, fatigue monitoring therefore relies on monitoring the loads and applying the known material properties, i.e. Wöhler curves, in accordance with the original design

https://doi.org/10.5194/wes-2026-133
Preprint. Discussion started: 30 July 2026

(DNV GL AS, 2025). Several solutions have been proposed using this concept, from direct measurement (Liu et al., 2025), using virtual sensing (Toftekær et al., 2023) and machine learning (de N Santos et al., 2023).

In load and lifetime monitoring, a recent topic of interest is the potential impact of curtailment on the residual lifetime of the asset. In this context, wind turbine curtailment is the deliberate reduction or complete shut-off of a wind turbine's electricity output, either requested by grid operators due to grid congestion or as part of ancillary service markets, or for commercial reasons such as pricing. Much variability exists in how curtailment is introduced, from rapid shutdowns to controlled set-point variations. Regardless of the motivation for curtailment, all curtailments introduce a new load cycle. This occurs because adjusting turbine power changes the thrust force and the resulting Fore-Aft (FA) bending moment. In particular, with partial curtailments, this introduces a load cycle that is similar to those typically induced by wind speed variations, Figure 1. It is these FA cycles that are of main interest in the current study.

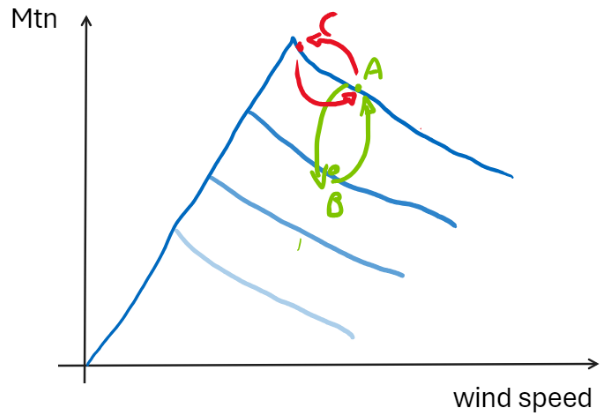

Figure 1. Conceptual drawing how operating a turbine under curtailment to different setpoints (here from A to B) introduces new low-frequency fatigue cycles (A-B-A) in the Fore-Aft bending moment M_{tn}, not to different from low-frequency fatigue induced from slow wind-speed variations (A-C-A) studied previously.

In this context, low-frequency fatigue dynamics (LFFD) should not be overlooked. In wind energy applications, this phenomenon occurs when load cycles cross the typical 10-minute time horizon, typically adopted in both design simulations and data collection. When properly accounted for, LFFD can contribute significantly to the overall fatigue life (Marsh et al., 2016; Sadeghi et al., 2023). In the current discussion, LFFD becomes relevant again, as slowly varying set-point variations in different curtailment strategies may easily span the typical 10-minute time horizon. Given the high dimensionality of the phenomenon, including wind speed, set-point variations and the reaction of the controller thereof, as well as the uniqueness of many curtailment scenarios, it is difficult to quantify the effect in a data-driven manner, especially when only limited SCADA is available (Santos et al., 2020). Meanwhile, while strain gauges have a proven track record of accurately capturing these LFFD loads (Sadeghi et al., 2023), they remain prone to failure and are labour-intensive to install, discouraging farmwide instrumentation. The installation of strain gauges is typically limited to a small subset of so-called *fleet leaders*.

https://doi.org/10.5194/wes-2026-133
Preprint. Discussion started: 30 July 2026

In this work, we investigate the use of more reliable accelerometers to provide a purely measurement-based way to monitor the effect of LFFD on wind turbines. The use of gravity-sensitive accelerometers for monitoring these loads is not novel, as others have suggested using it as part of a wider virtual sensing strategy (Thurn et al., 2026; Toftekær et al., 2023).

1.2 Farm wide monitoring using nacelle-mounted accelerometers

Operators increasingly aim to monitor all assets in a farm to cover local effects. This can be achieved by adopting a so-called fleet-leader strategy with a limited number of heavily instrumented turbines, combined with installing, for example, tri-axial MEMS accelerometers in the nacelle of all wind turbines. The latter allows measurements of accelerations in three orthogonal directions: parallel to the wind direction (fore-aft), perpendicular to the wind direction (side-side), and along the gravitational component. The primary use of these sensors is to measure vibrations and monitor resonance frequencies using Operational Modal Analysis (OMA), e.g. for scour monitoring (Magalhães and Cunha, 2011). Moreover, the acceleration data can also be used to infer the fatigue rates acting on the substructure via machine learning techniques (de N Santos et al., 2023), and even to reconstruct structural stress states through the aforementioned virtual sensing approaches (Toftekær et al., 2023). However, the focus still lies on the standard 10-minute time horizon. A complementary approach is therefore sought, in which a dedicated solution can serve operators to assess the impact of LFFD coming from curtailments, preferably with minimal additional data and modelling requirements and valid for each individual asset.

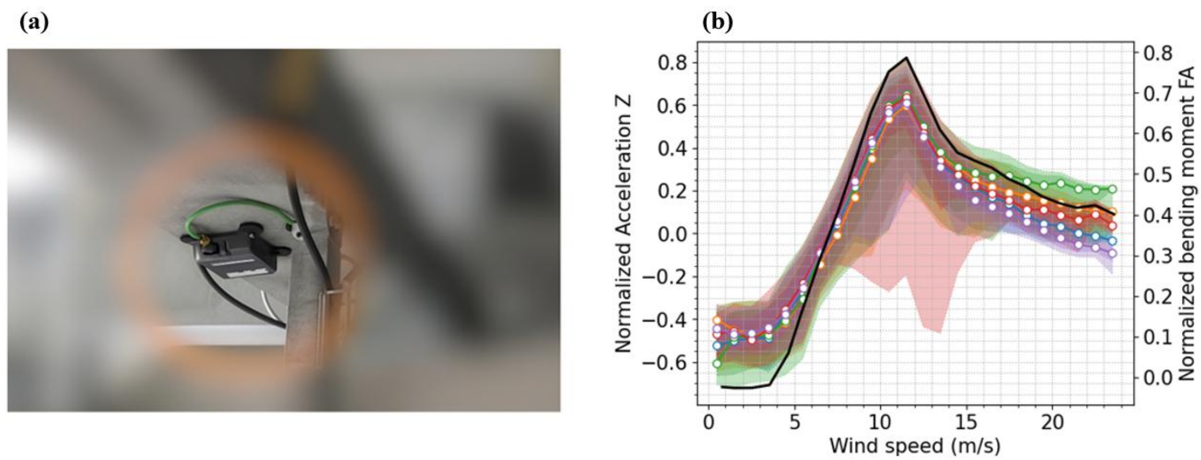

Figure 2. (a) MEMS accelerometer as installed in an offshore wind turbine (b) Z-direction acceleration measurement of the fleet leaders (multiple-coloured curves) as a function of wind speed, plotted together with bending moment (black curve) versus wind speed.

In this context, the MEMS accelerometers placed in the nacelle can be utilized to infer the nacelle's quasi-static rotations. This is possible because MEMS accelerometers are sensitive to gravity. Inferring rotations from MEMS accelerometers is common practice in many applications, most visibly in smartphones and drones. As such, roll and tilt/pitch angles can be readily inferred from MEMS accelerometer data. Note that yaw, the rotation around the vertical, cannot be

https://doi.org/10.5194/wes-2026-133
Preprint. Discussion started: 30 July 2026

eawe european academy of wind energy
Open Access WIND ENERGY SCIENCE DISCUSSIONS

inferred without an additional measurement, typically a magnetometer. As the rotation of the nacelle results from the flexible response to the loads it is subjected to, it can be hypothesized that the turbine loads can be inferred from observed rotations, Figure 2.

While the problem posed is seemingly trivial, there are some practical constraints one needs to be aware of when installing MEMS accelerometers in a farm of offshore wind turbines. In theory, when at rest, the accelerometers only measure the gravitational acceleration. However, this does not imply that when the turbine is at rest, the sensor is perfectly level. Especially when installation is done in quick succession, with fairly large tolerances, sensor installation offsets are to be expected, and these will be unique for each location.

Moreover, for an offshore wind turbine, some degree of tilt is always present due to the permanent tilt of the structure as a result of the monopile's installation tolerances and, to a lesser extent, foundation settlement or permanent structural deformation. Again, these installation tolerances will be unique for each location and can be considered as an additional offset. Meanwhile, the thrust-induced rotations should be fairly consistent in a fleet of similar structures and should be dictated by the turbine's operation.

The current paper proposes a methodology that results in a farmwide consistent estimate of the thrust-induced tilt by calibrating all individual sensors based on long-term monitoring data. Once calibrated and corrected, the rotations are transformed into an estimate of bending moment. Focusing on LFFD, this bending moment can be used to estimate stress and perform cycle counting on the long-term time series for fatigue analysis.

2 Methodology

2.1 Site and data description

The current work relies on data collected from a fully operational offshore wind farm situated in the North Sea. The turbines are from the 7 to 10 MW generation and are installed on XL-monopiles at moderate water depths. As such, the farm is representative of a significant part of the European offshore wind fleet.

The wind farm has adopted a fleet-leader strategy featuring approximately 10% heavily instrumented turbines. It currently already has a farmwide load monitoring strategy in place (De N Santos et al., 2024) to provide 10-minute fatigue rates. This study focuses on the nacelle accelerometer that is installed in every turbine in the farm. In an effort to minimize overhead, these accelerometers were installed by hand by the operator without a dedicated mounting bracket. Although time-efficient, this introduces a significant installation tolerance. Moreover, the sensors were installed on an oblique surface inside the nacelle. An additional offset linked to the angle of the oblique surface is introduced. Despite best attempts, the operator was not able to find any design drawings of the internals of the nacelle, and the offset introduced by the oblique surface can be considered an additional unknown common to all turbines.

In the current study, two datasets from the site are considered. An initial calibration dataset, from 01/01/2024 to 01/05/2025, is used to determine the offsets of all individual sensors and to establish a bending moment estimation using the

https://doi.org/10.5194/wes-2026-133
Preprint. Discussion started: 30 July 2026

fleet leaders. A second, shorter dataset from 03/04/26 to 10/04/26, from one of the fleet leaders, is used for validation. Interestingly, this relatively short dataset contains several curtailment events, Figure 3. Especially in the bending moment vs. power plot, the additional load cycles that come from curtailments are visible.

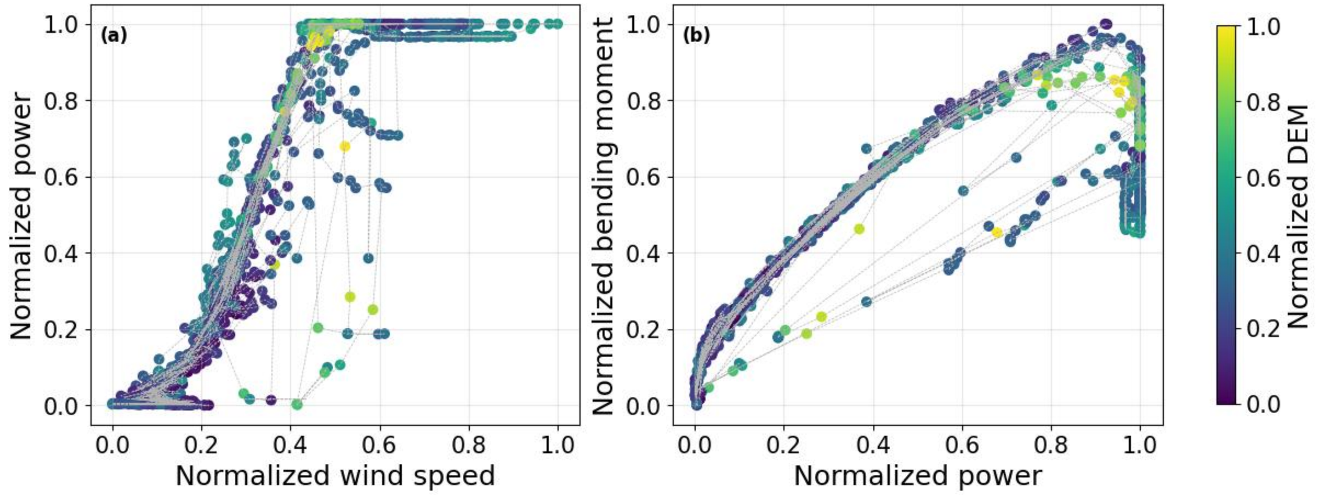

Figure 3. Illustration of the second validation dataset, taken from one of the fleet leaders. (a) power vs wind speed (b) Bending moment vs power with the colour scheme indicating the normalized DEM during the associated 10-minute interval and the lines indicating the sequence of the measured points

2.2 Low-frequency fatigue monitoring using nacelle accelerometers

The proposed solution for FA fatigue monitoring relies on using the three axes of the nacelle accelerometer to compute two rotations of the accelerometer in the global coordinate system, its pitch and roll. This assumes that the tower flexible deformation and subsequent rotation of the nacelle under loading are observable from the nacelle-mounted acceleration. This assumption was readily confirmed from the simple prior assessment in Figure 2, where simply looking at the mean value of the vertical (Z) axis of the accelerometer shows a strong correlation with the bending moment curve measured at the Tower-Transition Piece (TW-TP). However, significant scatter remains, which could later be falsely interpreted as load cycles and therefore needs to be eliminated.

At the root of this scatter lies the fact that a 0° measured inclination does not imply that the structure is without load, nor that a 0.1° inclination necessarily implies that the turbine is subjected to any load. This is due to two key offsets. The first, most trivial offset, is the sensor installation offset due to a relative rotation of the sensor with respect to the plane defined by the yaw platform, resulting in two angles, respectively rotated along the FA and SS axes. Simply because the surface on which the sensor is mounted is not perfectly flat, or is even significantly oblique, a practical mounting location might not be horizontal relative to the nacelle's bottom. As mentioned before, the details of this mounting location might not be known up front, as detailed design drawings of nacelle internals are not widely available. In part, this offset is common due to the common design of the nacelle, and in part it will differ per location due to installation tolerances in both the sensor and the nacelle. For simplicity, these offsets are considered time-independent. However, one must acknowledge that the sensor might creep over

https://doi.org/10.5194/wes-2026-133
Preprint. Discussion started: 30 July 2026

eawe european academy of wind energy
Open Access WIND ENERGY SCIENCE DISCUSSIONS

time or be disturbed, changing these offsets. The third offset, a relative yaw between the nacelle and the sensor, cannot be resolved afterwards and should be avoided during installation; it is assumed to be 0°.

A second offset comes from the tower itself, which will be tilted into a permanent direction as a result of the verticality tolerances during installation, with 0.25° typically employed as an upper limit. This tower tilt can be expressed using two angles: the magnitude of the permanent tilt, which is given by the pitch angle, and its corresponding heading from true north. As a result, the plane of rotation of the nacelle changes when the turbine yaws, and the sensor will rotate in this tilted plane. This results in a yaw-dependent projection of gravity, making both pitch and roll dependent on yaw. Again, these quantities are considered turbine-specific but time-independent, ignoring long-term settlement. Should such settlement occur, these components can still be updated accordingly.

Finally, the only two remaining rotations are the pitch and roll of the nacelle, respectively $\psi_{nacelle}$ and $\emptyset_{nacelle}$. Exactly these components are linked to the flexible deformation of the tower under thrust load. With $\emptyset_{nacelle}$ linked to sideways loads, our main interest lies with the $\psi_{nacelle}$ which will vary under thrust loading.

The proposed low-frequency monitoring strategy therefore comprises the following steps:

- Estimation of the sensor offset ψ_{offset} ,$\emptyset_{offset}$ and permanent turbine tilt ψ_{Tower} , θ_{Tower}, using long-term data, for each individual turbine, Section 3.
- Estimation of the FA bending moment from the normalized pitch angle and known turbine yaw using the fleet leaders as guidance, Section 4.
- Long term cycle counting on the low-frequency fatigue data, Section 5

In the remainder of the manuscript, these three steps will be explained, showing the intermediary results attained from the monitoring dataset introduced in Section 2.1.

3 Sensor offset and permanent tilt estimation

3.1 Methodology

The methodology used to estimate the sensor offset and permanent tilt was detailed in (Chaar et al., 2026) and is summarized here.To isolate the sensor offset and tower tilt from the natural variability due to loads, parked conditions can be considered. However, during parked conditions, eccentric loading is present because the center of gravity of the rotor-nacelle assembly is offset from the tower axis. As an additional constraint, the data are filtered below the cut-in wind speed, between 3.6 m/s and 3.9 m/s, using for example the wind speed from SCADA, where horizontal wind loading counteracts the eccentric loading of the structure. At this filtered windspeed, the fleet is idling due to low wind speed. It is then assumed that the pitch and roll of the nacelle are in their zero-load state and that only sensor offset and tower tilt remain.

At this stage, the nacelle position, or yaw, as obtained for example from SCADA, is essential to estimate the permanent tilt angles. Simply put, the yaw angle at which the accelerometers record the largest pitch angle aligns with the

https://doi.org/10.5194/wes-2026-133
Preprint. Discussion started: 30 July 2026

heading of the permanent tilt. For other headings, a sinusoidal relationship exists in the observed mean accelerations and the difference between the continuously varying yaw angle and the constant heading of the permanent tilt. The amplitude of this oscillation is dictated by the magnitude of the tilt.

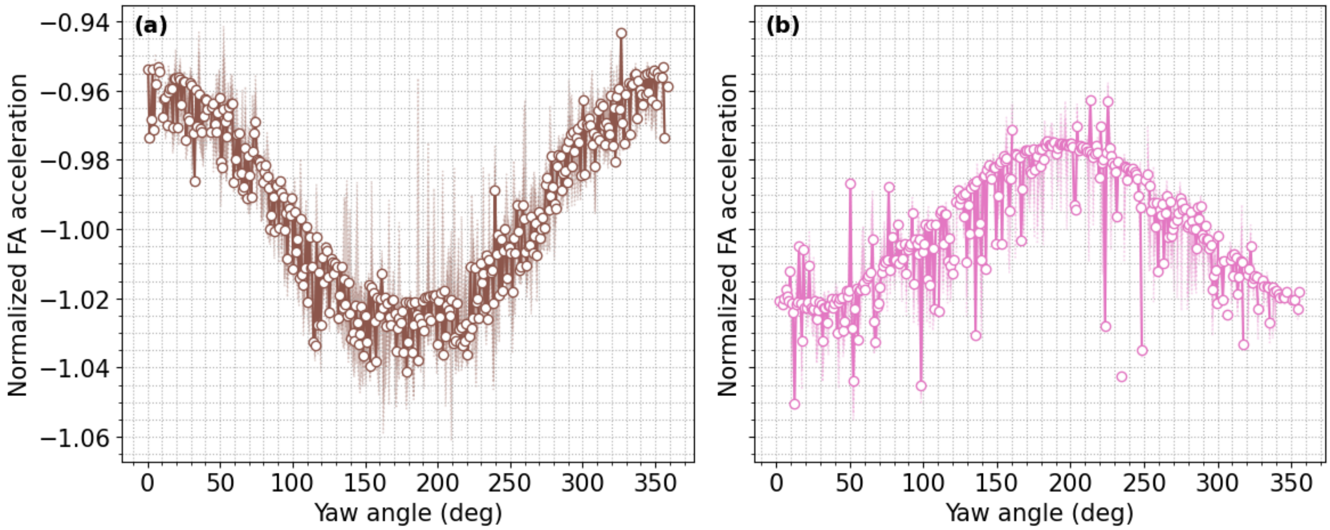

Figure 4. Exemplary data from two locations, showing the variability in mean acceleration for different yaw angles, depending on the severity of the turbine tilt and sensor offset. (a) Turbine 33: the highest tower tilt in the farm. (b) Turbine 6: a turbine with an average tower tilt

For instance, when the tower is not tilted, there is no influence of the yaw angle, and the oscillation amplitude is zero. In other words, the phase and amplitude of the measured pitch-angle variation with respect to yaw provide an estimate of the turbine's permanent tilt. Meanwhile, the sensor offsets shift the mean value of the acceleration in each direction and thus the zero offset of the aforementioned oscillation. Figure 4 illustrates this phenomenon, with Turbine 33 (a) having the highest computed tower tilt, while Turbine 6 (b) corresponds to a turbine with intermediate tower tilt in the wind farm. The tower tilt is proportional to the amplitude of the sinusoid. Another interesting observation is that each turbine reaches its maximum at a different yaw angle, as the tilt direction differs between turbines. Finally, a slight variation in sensor offset can be observed among the turbines, as indicated by the different vertical positions of the sinusoidal curves. In particular, the sinusoid corresponding to Turbine 6 is centered at a slightly higher value, indicating a higher sensor offset.

3.2 Results

The methodology described in (Chaar et al., 2026) was applied to an entire wind farm, and the farmwide permanent tilt and heading angles are shown in Figure 5, together with the estimated sensor offsets for pitch and roll. In particular, note the scatter in the permanent tilts; as expected, this effect is highly localized. Meanwhile, the farmwide sensor pitch angles mostly align around 6°, which one design drawing confirmed to be the angle of the oblique mounting surface. It is worth noting that the

https://doi.org/10.5194/wes-2026-133
Preprint. Discussion started: 30 July 2026

variability between turbines is significant and exceeds the values of the permanent tilt, which are all below 0.25°. The roll angle is scattered around 0° and again shows a significant amount of scatter. The scatter in both sensor pitch and roll is likely linked to tolerances in the mounting of the sensor using screw-on magnets and variability in the mounting surface.

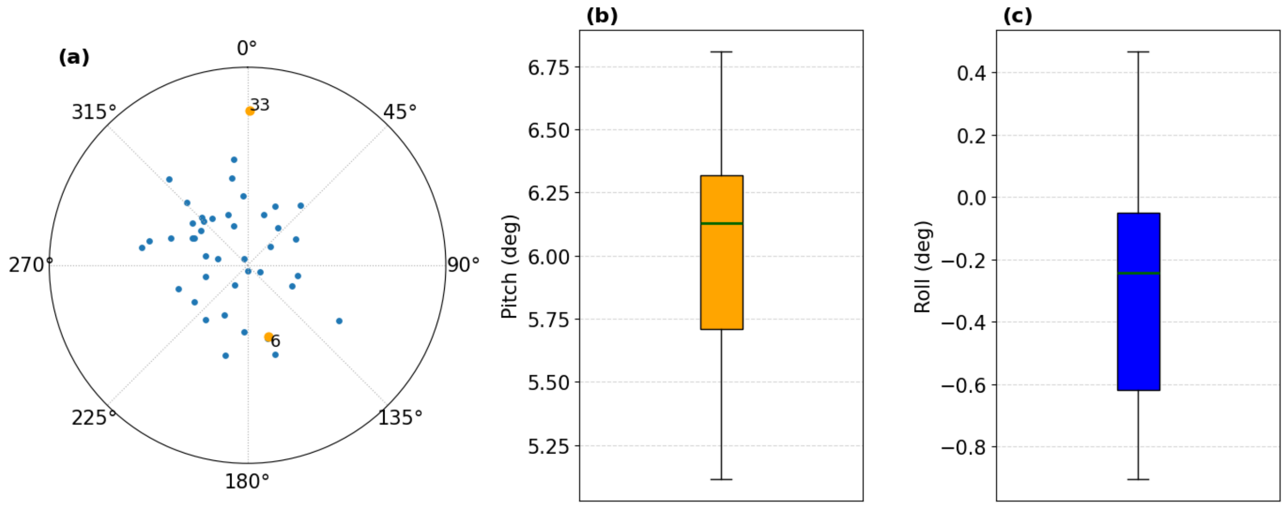

Figure 5. (a) Farm wide permanent tilt, locations 6 and 33 are highlighted in orange. (b) Farm-wide estimated sensor pitch angles. (c) Farm-wide estimated sensor roll angles.

4 Load and Bending moment estimation

4.1 Methodology

To estimate the load characteristics of the nacelle, the previously identified offsets affecting the tri-axial sensor measurements must be eliminated, starting with the sensor offsets, which are accounted for using a standard rotation matrix. The governing equations of the system once the sensor offset is accounted for can be written as:

$$\vec{\boldsymbol{a}}^{c}{}_{\boldsymbol{mean}} = R_s{}^{-1}\vec{\boldsymbol{a}}_{\boldsymbol{mean}} = R_n\, R_t\vec{\boldsymbol{g}} \tag{1}$$

With R_s being the sensor offsets rotation matrix , R_n the nacelle load characteristic matrix and R_t the tower-tilt matrix. Here, the tower-tilt matrix describes the sinusoidal behavior seen in the data due to the permanent tower tilt, while the load matrix describes the load characteristic acting on the nacelle and projecting onto the sensor. Because rotation matrices are not commutative, the tower influence is not separable via inverse rotation. Multiplying the tower matrix with the gravity vector $\vec{\boldsymbol{g}}$ gives:

$$\vec{\boldsymbol{t}} = R_t\vec{\boldsymbol{g}} = R_z\,(\theta_{nacelle} - \theta_{Tower})R_y(\psi_{Tower})R_z(\theta_{Tower})\vec{\boldsymbol{g}} \tag{2}$$

https://doi.org/10.5194/wes-2026-133
Preprint. Discussion started: 30 July 2026

$$\vec{\boldsymbol{t}} = \begin{bmatrix} f_x(\psi_{Tower}, \theta_{tower}, \theta_{nacelle}) \\ f_y(\psi_{Tower}, \theta_{tower}, \theta_{nacelle}) \\ f_z(\psi_{Tower}) \end{bmatrix} \tag{3}$$

The remaining unknowns are the load-induced roll and pitch of the nacelle. The matrix describing the nacelle characteristics is given by:

$$R_x(\emptyset_{nacelle})R_y(\psi_{nacelle}) = \begin{bmatrix} \cos\psi_{nacelle} & 0 & \sin\psi_{nacelle} \\ \sin\psi_{nacelle}\sin\emptyset_{nacelle} & \cos\emptyset_{nacelle} & -\sin\emptyset_{nacelle}\cos\psi_{nacelle} \\ -\cos\emptyset_{nacelle}\sin\psi_{nacelle} & \sin\emptyset_{nacelle} & \cos\psi_{nacelle}\cos\emptyset_{nacelle} \end{bmatrix} \tag{4}$$

This matrix is nonlinear, and multiplying it with tower-tilt vector $\vec{\boldsymbol{t}}$ results in nonlinear equations that are complex to solve and do not have a unique solution. However, if small angles are assumed, the following substitutions can be made:

- $\sin\psi_{nacelle} = \psi_{nacelle}$ *and* $\sin\emptyset_{nacelle} = \emptyset_{nacelle}$
- Second-order terms are considered to be significantly lower in magnitude than first-order terms.
- $\cos\psi_{nacelle} = 1$, $\cos\emptyset_{nacelle} = 1$ and $f_z(\psi_{Tower}) = -1$

This results in:

$$\vec{\boldsymbol{a}}^c = R_n\vec{\boldsymbol{t}} = \begin{bmatrix} f_x(\psi_{Tower}, \theta_{tower}, \theta_{nacelle}) - \psi_{nacelle} \\ f_y(\psi_{Tower}, \theta_{tower}, \theta_{nacelle}) + \emptyset_{nacelle} \\ -1 - \psi_{nacelle} * f_x(\psi_{Tower}, \theta_{tower}, \theta_{nacelle}) + \emptyset_{nacelle} * f_y(\psi_{Tower}, \theta_{tower}, \theta_{nacelle}) \end{bmatrix} \tag{5}$$

Under these assumptions, the rotation of interest is fully decoupled from the tower's permanent tilt, requiring only the turbine yaw to be known. It is sufficient to subtract these final contributions from the FA accelerations; the pitch characteristic is then given by:

$$\psi_{nacelle}(\mathrm{t}) = f_x(\psi_{Tower}, \theta_{tower}, \theta_{nacelle}) - \overline{a_x^c}(\mathrm{t}) \tag{6}$$

The final step is to transform the measured nacelle pitch angles into an estimate of bending moment, in which $\overline{a_x^c}(\mathrm{t})$ is the mean acceleration in the x direction in the associated 10 minute window t. This can, in principle, be done using a simple finite-element model of the structure. However, when fleet leaders are available, a purely data-driven methodology can be employed. As the relationship between bending moment and nacelle pitch is assumed to be linear, a simple linear model can be fitted to the data to perform the final mapping.

$$M_{tn}(t) = A\,\psi_{nacelle}(t) + B \tag{7}$$

Here, A represents the slope and B represents the offset term, both estimated using linear regression on long-term 10-minute mean data.

https://doi.org/10.5194/wes-2026-133
Preprint. Discussion started: 30 July 2026

4.2 Results

The load characteristics across the farm are presented in Figure 6. The load characteristics of all turbines have a similar shape, which aligns with the expectation that inclination depends on load and that turbines will behave similarly under similar conditions. Some spread remains, which is linked to turbine-specific attributes, as substructure designs vary across the farm. From the shaded areas, one can also see that turbines deviate from these nominal values, mostly due to local curtailment.

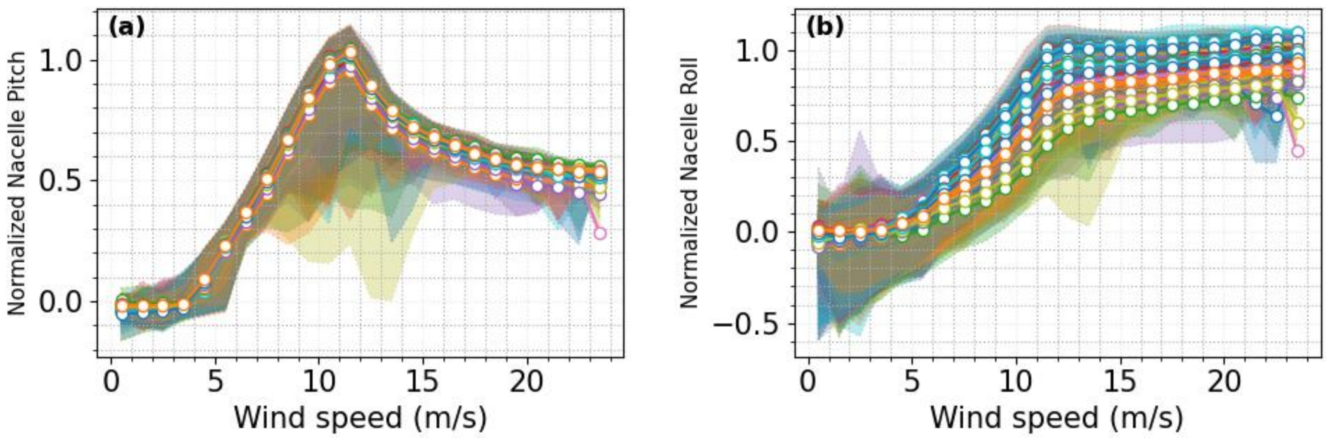

Figure 6. (a) Normalized nacelle pitch angle (b) Normalized nacelle roll angle, with the lines indicating the medium value, The shades are the 10th and 90th percentile respectively.

The final linear model linking nacelle pitch to fore-aft bending is trained using data from two fleet-leader turbines, turbines 1 and 2. One turbine is used for training, and the other is used for validation and tuning. The remaining turbines, turbines 3, 4 and 5, are used to evaluate the model on unseen data and assess its ability to generalize. One would expect that, under similar loading, the turbines would behave similarly. Nevertheless, these turbines differ in both design and boundary conditions, such as water depth. Hence, the model evaluation also serves to quantify the impact of these differences on predictive performance across the farm.

To evaluate the model, mean absolute error (MAE) and coefficient of determination (R^2 score) are used. R^2 quantifies the correlation between predicted and measured bending moments, while MAE expresses the error relative to the normalized data. As an additional benchmark for the simple linear regression, which requires no additional SCADA, a more complex XGBoost model is used, with a total of five SCADA parameters: rotor pitch, rotor speed, yaw, wind speed and power. The objective is to assess whether there is any added value in using such a complex model over a simpler linear model and to assess whether any relationships were overlooked. Only if XGBoost significantly outperforms the linear model could one argue that more advanced solutions are required.

The results are presented in Figure 7 and Table 1, respectively. The results show that XGBoost outperforms linear regression on the training and testing turbines, except for turbine 3. For the XGBoost model, the performance fluctuates between an MAE of 0.93% and 3.74%, with the performance on turbine 5 closely resembling that of the training turbines,

https://doi.org/10.5194/wes-2026-133
Preprint. Discussion started: 30 July 2026

which could be attributed to similar boundary conditions. By contrast, the linear regression maintains a more consistent output, with an average MAE of 3.5%. For both models, a strong correlation between the predicted and measured bending moment is observed, indicating that the mapping was successful regardless of the model used. Although XGBoost has 0.85% less error than the simpler linear model overall, the linear regression generalizes better across the fleet. Hence, the linear model provides a more robust and interpretable baseline for mapping nacelle motion to structural bending response. In addition, the linear model depends on only one input, eliminating the need for any further SCADA collection beyond the yaw angle. Both models maintained similar error levels after deployment from 01/01/2025 onwards, indicating stable predictive performance over time.

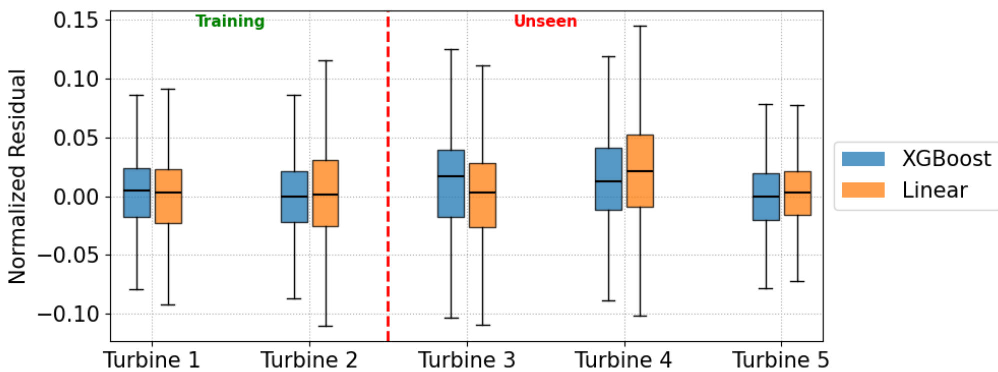

Figure 7. The residual of the two models, trained on Turbine 1 and 2, defined as measured bending moment subtracted from the predicted bending moment. The training periods spans from 01/01/2024 – 01/01/2025.

Table 1 Linear model and XGBoost evaluation metrics for the period 01/01/2024 – 01/01/2025. The red line separates the training turbines from the testing turbines.

Turbine	1	2	3	4	5
MAE LINEAR	3.02	3.59	3.41	4.38	2.91
MAE XGBOOST	2.78	0.93	3.74	3.10	2.54
R2 Linear	0.98	0.97	0.98	0.96	0.98
R2 XGBoost	0.99	0.99	0.98	0. 98	0.99

5 Low frequency fatigue monitoring

5.1 Methodology

The objective of the current study is to evaluate whether it is feasible to use the nacelle-mounted accelerometer to monitor LFFD as a surrogate for a bending moment computed from a strain gauge measurement, e.g. at the TW-TP interface. As shown

https://doi.org/10.5194/wes-2026-133
Preprint. Discussion started: 30 July 2026

in the previous sections, it is relatively straightforward to replicate the quasi-static bending moments from the accelerometer's mean accelerations.

However, to prove useful, we need to understand whether all relevant low-frequency fatigue can be captured properly from the nacelle accelerometer without any additional processing or corrections. There is no specific definition of what constitutes LFFD, but as a logical rule we consider all effects at frequencies below the lowest cyclic loads, namely the 1P rotor harmonic and wave loading. In this study, we adopt a fourth-order Butterworth low-pass filter at 0.08 Hz. To compare the methodologies, both the bending-moment time signal and the nacelle-accelerometer signal are filtered. This upper bound is sufficiently high to capture turbulent wind, as well as set-point variations in the controller. However, it is beyond what can be accurately described with industry-standard 10-minute SCADA.

Note that, when predicting bending moments from the accelerometer, the yaw angle is required. As this is obtained from SCADA as a 10-minute average, the yaw angle is artificially fixed. This introduces an error when the yaw angle changes significantly within a 10-minute window.

To properly account for long-term cycles, the time-series data need to be considered as one continuous time series rather than being cut into 10-minute blocks. In the current study, which uses only a limited duration of one week, the filtered data are concatenated into one continuous time series. Missing data points in either source were handled by removing the corresponding timestamp from both series. Alternatively, a method using residual recovery, as proposed in (Marsh et al., 2016) and implemented in py-fatigue (D'Antuono et al., 2023), would have worked equally well and would be more efficient for long-term monitoring. The concatenated time series of both the measured and estimated bending moments are translated into stress using the relationship in Equation 8.

$$\sigma_{tn}(t) = \frac{M_{tn}(t) * R_o}{I} \tag{8}$$

Here, the radius term is the outer radius of the tower, I is the second moment of area, and the stress and bending-moment terms correspond to the FA direction. Both the estimated and measured bending-moment time series were processed using py-fatigue to compute the fatigue spectrum and damage-equivalent moments (DEM) for different Wöhler exponents.

5.2 Results

The stress time series are computed and plotted together with the residual, as presented in Figure 8. As shown in the figure, overall, the model trained on 10-minute intervals can predict the data sufficiently well, with the margin of error remaining within MAE of 2.6%. The error is highest during parked conditions (green), during which the accelerometer still predicts variability in the load that is not reflected by the strain measurements at the TP-TW interface. Cyclic behaviour is observed in the accelerometer output as the turbine continues to yaw during this period. The explanation is straightforward: the model trained to link nacelle tilt to bending moment assumes lateral thrust loading on the rotor. However, during idling, this load is

https://doi.org/10.5194/wes-2026-133
Preprint. Discussion started: 30 July 2026

absent, and what remains is the deadweight of the RNA, so the previously fitted relationship between bending moment and nacelle pitch breaks down.

One could argue that the role of LFFD during parked is negligible, as is most visible from the nearly constant measured bending moments. In practical applications, one could assume it is therefore sufficient to discard parked conditions or consider the signal as constant. Nonetheless, introducing a more correct representation during parked conditions might still be desirable, in particular as it could lie at the root of the overestimation of negative bending moments for normalized stresses below 0.

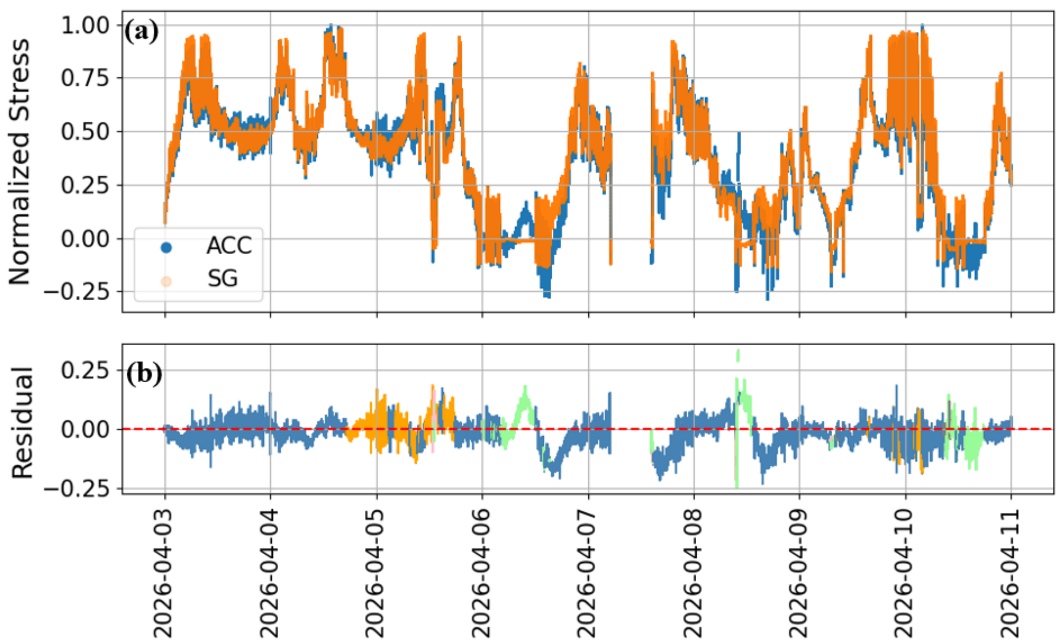

Figure 8. (a) Estimated low frequency stress using the accelerometer (in blue) and measured stress (orange) (b) residual of predicted stress minus the measured stress with the colour scheme indicating turbine states: standstill (green) , nominal (blue) , derated (orange) and (pink) start-stop events

The resulting rainflow-cycle-count histograms for both signals are shown in Figure 8. The figure shows stress range (MPa) plotted against cumulative cycle count (N). Most loading cycles are concentrated at low stress ranges, below 0.2, while high-stress-range cycles occur less frequently but contribute significantly to the accumulated fatigue damage. Although there is adequate agreement across different stress ranges for both the accelerometer and strain-gauge methods, noticeable differences are still present. The accelerometer-based estimate reaches a 1.13 higher stress range than the strain gauges, with 1 cycle not being present in the strain gauges measurements. Moreover, in most cases, the accelerometer-based strategy overestimates the number of cycles in particularly for stress range below 0.2, where the cycle count is almost twice the number of cycles from the strain gauges. This is mostly attributed to the mismatch in the negative normalized stress between the trained linear model and the measured data, or to rapidly changing yaw angles within a 10-minute window, where yaw was assumed to be fixed. Thus, factors such as modelling error, limitations in the input variables, and noise contribute to additional cycles.

https://doi.org/10.5194/wes-2026-133
Preprint. Discussion started: 30 July 2026

Despite the difference observed in the cycle count, the damage estimated from the accelerometer is proportional to the damage measured with the strain gauges. The damage-equivalent moment (DEM) was subsequently computed for different values of the Wöhler exponent using the bending moments obtained from both systems. The results are presented in Table 2. The estimated DEMs show good agreement with the measured values, with the mean absolute percentage error (MAPE) remaining below 10% for all cases. Although the RMSE increases with increasing Wöhler exponent, reflecting the larger weighting of high-amplitude load cycles in the fatigue calculation, the consistently low MAPE indicates that the proposed regression model accurately reproduces the fatigue-relevant loading. However, improvements should still be made to fully replace the role of the strain gauges.

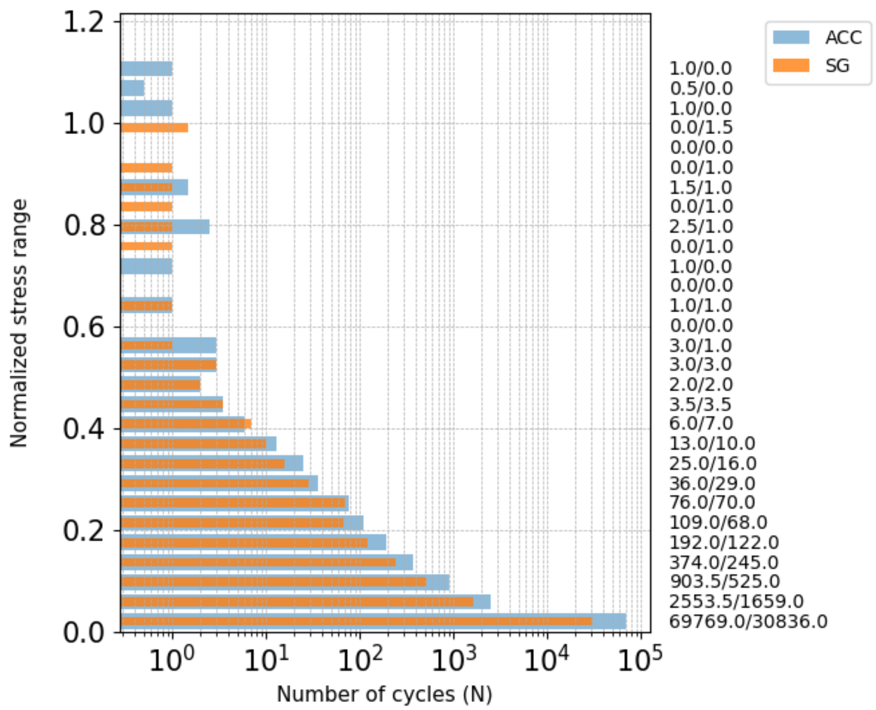

Figure 9. Cycle count of the estimated and measured stress from the accelerometer and strain gauge respectively. The exact cycle count number is shown on the right of the figure: accelerometer/strain cycles.

https://doi.org/10.5194/wes-2026-133
Preprint. Discussion started: 30 July 2026

Table 2 Normalized DEM (taking Measured DEM for m=3 as basis) of both the accelerometer and the strain gauges. MAPE and RMSE are used for evaluating the estimated Dem from accelerometer with respect to measured one from strain gauges.

m	Measured DEM	Estimated DEM	MAPE (%)	RMSE
3	1	1.09	9.89	0.09
4	2.67	2.90	8.61	0.23
5	5.11	5.56	8.81	0.45

6 Conclusion

The current paper investigated the feasibility of using a nacelle-mounted DC-capable accelerometer in offshore wind turbines to estimate low-frequency fatigue dynamics (LFFD) and its resulting impact on loading. In particular, the study focuses on mitigating the impact of installation tolerances in these sensors and the impact of permanent tower tilt. A simple procedure to estimate these offsets and account for them, using solely a yaw angle obtained from SCADA, was proposed.

After *calibration*, inter-turbine differences are largely mitigated, and consistent estimates of both pitch and roll angles are obtained. The nacelle angles were then linked to the bending moments obtained from the fleet leaders via a simple linear regression. A comparison with a more complex XGBoost model, including additional SCADA inputs, did not yield any significant improvement, suggesting that the nacelle accelerometer alone captures the relevant variability. However, final results suggest that in future improvements parked conditions should be treated differently.

The stresses obtained from both setups were then used to evaluate damage occurring on a fleet-leader turbine during a one-week period covering various operating conditions. The accelerometer-based estimation resulted in good agreement in predicting the total DEM compared with the strain-gauge-based method, with the margin of error remaining below 3%. This agreement was achieved despite false accelerometer predictions during parked conditions and a larger number of smaller cycles.

The current methodology leaves room for improvement, but these results demonstrate the feasibility of obtaining a reasonable estimate of LFFD effects in the short term.

Author contributions. Conceptualization: M.C. and W.W. Methodology: M.C. and W.W. Funding acquisition: C.D. Data visualization: M.C. and W.W. Writing original draft: M.C. and W.W. All authors approved the final submitted draft.

Data availability. The data used in this study cannot be made publicly available. The acceleration data, SCADA data, and strain gauge measurements were provided by an industrial partner under a confidentiality agreement and are therefore not available for public release.

https://doi.org/10.5194/wes-2026-133
Preprint. Discussion started: 30 July 2026

Acknowledgments. This work was supported by the Flanders Innovation & Entrepreneurship agency (Project VLAOO23).

Funding statement. This research was funded by the Flanders Innovation & Entrepreneurship agency (Project VLAOO23).

Ethical standard. The research meets all ethical guidelines, including adherence to the legal requirements of the study country.

7 Bibliography

Chaar, M., Weijtjens, W., and Devriendt, C.: Fleetwide Detection of Tower Tilt and Nacelle Load Characteristics Using Tri-Axial Accelerometer Measurements, 2026.

D'Antuono, P., Weijtjens, W., and Devriendt, C.: OWI-Lab/py_fatigue: Zenodo registration, https://doi.org/10.5281/zenodo.7656681, 2023.

De N Santos, F., Noppe, N., Weijtjens, W., and Devriendt, C.: Farm-wide interface fatigue loads estimation: A data-driven approach based on accelerometers, Wind Energy, 27, 321–340, https://doi.org/10.1002/we.2888, 2024.

DNV GL AS: RP-C203: Fatigue design of offshore steel structures, 2025.

Liu, Q., Chang, S., Feng, G., and Liu, F.: Top displacement estimation for monopile-supported offshore wind turbine based on the combination of acceleration and inclination, Ocean Eng., 327, 120954, https://doi.org/10.1016/j.oceaneng.2025.120954, 2025.

Magalhães, F. and Cunha, Á.: Explaining operational modal analysis with data from an arch bridge, Mech. Syst. Signal Process., 25, 1431–1450, https://doi.org/10.1016/j.ymssp.2010.08.001, 2011.

Marsh, G., Wignall, C., Thies, P. R., Barltrop, N., Incecik, A., Venugopal, V., and Johanning, L.: Review and application of Rainflow residue processing techniques for accurate fatigue damage estimation, Int. J. Fatigue, 82, 757–765, https://doi.org/10.1016/j.ijfatigue.2015.10.007, 2016.

de N Santos, F., D'Antuono, P., Robbelein, K., Noppe, N., Weijtjens, W., and Devriendt, C.: Long-term fatigue estimation on offshore wind turbines interface loads through loss function physics-guided learning of neural networks, Renew. Energy, 205, 461–474, https://doi.org/10.1016/j.renene.2023.01.093, 2023.

Sadeghi, N., D'Antuono, P., Noppe, N., Robbelein, K., Weijtjens, W., and Devriendt, C.: Quantifying the effect of low-frequency fatigue dynamics on offshore wind turbine foundations: a comparative study, Wind Energy Sci., 8, 1839–1852, https://doi.org/10.5194/wes-8-1839-2023, 2023.

Santos, F. d N., Noppe, N., Weijtjens, W., and Devriendt, C.: SCADA-based neural network thrust load model for fatigue assessment: cross validation with *in-situ* measurements, J. Phys. Conf. Ser., 1618, 022020, https://doi.org/10.1088/1742-6596/1618/2/022020, 2020.

Thurn, J., Jonscher, C., Hofmeister, B., Zorzi, G., and Rolfes, R.: Virtual sensing for strain estimation in wind turbine support structures based on a single accelerometer, [preprint], https://doi.org/10.5194/wes-2026-5, 20 February 2026.

https://doi.org/10.5194/wes-2026-133
Preprint. Discussion started: 30 July 2026

Toftekær, J. F., Vestermark, J. T., and Jepsen, M. S.: Uncertainty of Virtually Sensed Stress Ranges in Offshore Wind Support Structures, in: Volume 1: Offshore Technology, ASME 2023 42nd International Conference on Ocean, Offshore and Arctic Engineering, V001T01A011, https://doi.org/10.1115/OMAE2023-101045, 2023.

Vorpahl, F., Schwarze, H., Fischer, T., Seidel, M., and Jonkman, J.: Offshore wind turbine environment, loads, simulation, and design: OWT loads and design, Wiley Interdiscip. Rev. Energy Environ., 2, 548–570, https://doi.org/10.1002/wene.52, 2013.

Wilkie, D. and Galasso, C.: Gaussian process regression for fatigue reliability analysis of offshore wind turbines, Struct. Saf., 88, 102020, https://doi.org/10.1016/j.strusafe.2020.102020, 2021.